Study of the crystal structure, phase composition and magnetic properties of textured magnetite films grown by reactive deposition

© V.V. Balashev[1,2], A.V. Shevlyagin[1], A.V. Prikhodchenko[2], D.A. Tsukanov[1,2], A.Yu. Samardak[2], M.I. Sobirov[2], A.V. Ognev[2,3], A.S. Samardak[2,3]

[1] Institute of Automation and Control Processes, Far East Branch, Russian Academy of Sciences,
Vladivostok, Russia
[2] Institute of High Technologies and Advanced Materials, Far Eastern Federal University,
Vladivostok, Russia
[3] Sakhalin State University,
Yuzhno-Sakhalinsk, Russia

E-mail: balashev@mail.dvo.ru

The study of magnetic films grown on the oxidized silicon surface is of interest from the point of view of creating „ferromagnetic metal/dielectric" tunnel contacts and implementing the transport of spin-polarized electrons. In this work, textured polycrystalline magnetite films were prepared by reactive deposition of iron onto a $SiO_2/Si(001)$ surface under a molecular oxygen atmosphere. Films with a thickness of $15-250$ nm were studied using Raman spectroscopy and X-ray diffraction. From the analysis of experimental data, it was established that as a result of reactive deposition, magnetite crystallites grow predominantly in two orientations — (311) and (100). The crystallite lattice constant does not depend on the film thickness, but its value is $\sim 1\%$ less than for single-crystal magnetite. Studies of magnetic properties have shown that the magnetic behavior of samples greatly changes its character in samples with a magnetite film thickness of less than 70 nm.

Keywords: magnetite, texture, silicon, reactive deposition, Raman spectroscopy.

DOI: 10.61011/PSS.2024.03.57937.265

1. Introduction

According to theoretical calculations, a semimetal such as magnetite (Fe_3O_4) may feature a 100% spin polarization of conduction electrons [1] and holds promise for application in spintronics as a material for devices utilizing the electron spin for data receiving, processing, and transfer [2]. It was noted that the Schottky barrier at the interface between a ferromagnetic material and a semiconductor may act as a tunnel barrier upon injection of spin-polarized electrons into the semiconductor [3]. „Ferromagnetic metal/dielectric" (Fe/SiO_2 [4], CoFe/MgO [5], Fe/MgO [6], etc.) tunnel contacts are used widely as injectors/detectors of spin-polarized electrons in studies into spin accumulation and spin transport in silicon. The results of an experimental study of spin accumulation in silicon [7] revealed that the use of a Fe_3O_4/MgO tunnel contact is preferable to Fe/MgO. A Fe_3O_4/SiO_2 contact with an ultrathin SiO_2 layer is no less promising than Fe_3O_4/MgO in terms of enhancing the efficiency of injection of spin-polarized electrons into silicon. Therefore, it is fair to say that both the synthesis of a high-quality (in terms of its structural and phase composition) magnetite film on the surface of oxidized Si and the examination of its electrical and magnetic properties are important. Miniaturization of modern electronic components necessitates the application of films that retain their magnetic and electrical properties in the course of size

reduction. In view of this, it is important to choose the range of thicknesses within which the films would have optimum characteristics needed for a given device structure.

We have demonstrated in our earlier studies [8,9] that a polycrystalline magnetite film with a preferred crystallite orientation grows when iron is deposited onto the surface of an ultrathin SiO_2 layer in an oxygen atmosphere. The relation between magnetotransport properties of magnetite films and their thickness was established. The examination of structural properties was limited to analyzing the growth surface of Fe_3O_4 films by reflection high-energy electron diffraction (RHEED). Diffraction patterns are formed in this method as a result of scattering of electrons incident under grazing angles on the film surface ($\sim 0.5-3°$). Large islands protruding above the film surface produce the primary contribution to electron diffraction. The analysis of RHEED patterns revealed [9] that crystallites have a preferred (311) orientation within the $15-250$ nm thickness range of films. At the same time, RHEED does not provide a conclusive answer to the question regarding the possible presence of crystallites of a different orientation. In the present study, textured magnetite films with a thickness of $15-250$ nm were fabricated, and the variation of their phase composition with thickness was examined by Raman spectroscopy. X-ray diffraction analysis was also performed to determine the structural properties of films.

2. Procedure of sample synthesis and investigation

Magnetite films were synthesized on an oxidized silicon surface in a „Katun" ultrahigh-vacuum chamber with a base pressure of $1 \cdot 10^{-10}$ Torr fitted with instruments for RHEED (Omicron RH 20 S) and spectral ellipsometry (Ellipse-1891 SAG). In these experiments, iron was evaporated thermally from a Knudsen cell at a rate of 2.5 nm/min. Molecular oxygen was introduced into the vacuum chamber in the process of deposition of Fe onto the $SiO_2/Si(001)$ surface at a temperature of $300°C$. The partial oxygen pressure in the course of iron oxide film growth was $3 \cdot 10^{-6}$ Torr. RHEED patterns and data on the crystal structure could be retrieved in the process of growth. The thickness of an iron oxide film could be determined by ellipsometry immediately after the deposition. The film thickness range examined in the present study was $15-250$ nm. Wet chemical processing [10] was used to clean the surface of Si and form an ultrathin (approximately 1.5 nm) SiO_2 layer on it.

Raman spectra were recorded by an NTEGRA Spectra II (NT-MDT, Russia) measurement system at room temperature within the $150-1000$ cm^{-1} frequency range under excitation at a wavelength of 473 nm. The film structure was examined by X-ray diffraction with a COLIBRI portable XRD system (Bourevestnik JSC, Russia) diffractometer. Magnetic properties were determined using a VSM 7410 (LakeShore, USA) vibrating sample magnetometer.

3. Experimental results and discussion

Figure 1 presents Raman spectra from the surface of polycrystalline Fe_3O_4 films of various thickness. It is evident that the measured Raman spectrum changes completely as the thickness increases from 15 to 250 nm. The Raman spectra of thick films feature peaks at the frequencies of 308, 538, and 667 cm^{-1}, which agree closely with the positions of magnetite peaks in a Raman spectrum. It is known that the magnetite spectrum [11] is characterized by three active Raman T_{2g}-modes at 193, 308, and 540 cm^{-1} and one active A_{1g}-mode at a frequency of 670 cm^{-1}. The peak at a frequency of 193 cm^{-1} has a low intensity and was not observed in the present study. The positions of peaks for grown films also agree well with the values of 306, 538, and 668 cm^{-1} derived from the spectrum of a natural bulk magnetite sample [12].

Raman peak A_{1g}, which becomes well-pronounced when the thickness of deposited magnetite exceeds 35 nm, is the most intense in the magnetite spectrum. Its position (approximately 666.5 ± 0.5 cm^{-1}) remains essentially unchanged throughout the entire thickness range. Measurements of the full width at half maximum (FWHM) of peak A_{1g} demonstrated the film thickness does also exert only an insignificant influence on this quantity. The FWHM
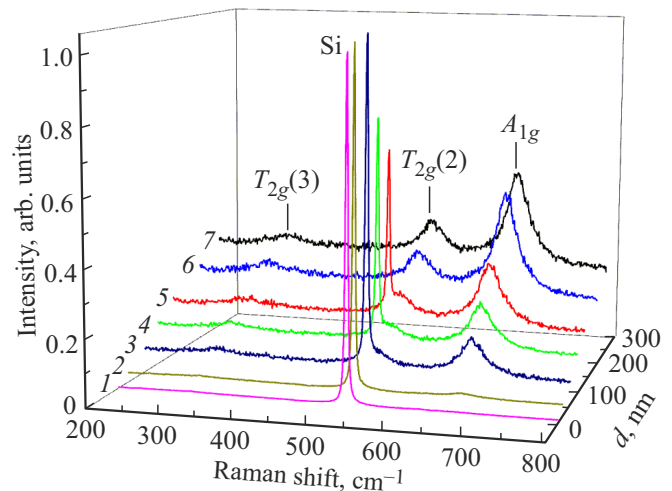
Figure 1. Raman spectra measured at different magnetite film thicknesses: *1* — 15 nm, *2* — 35 nm, *3* — 70 nm, *4* — 100 nm, *5* — 135 nm, *6* — 200 nm and *7* — 250 nm.

value was 40 cm^{-1}, which agrees closely with the data for crystalline magnetite ($\sim$ 39 [11]), an epitaxial 150-nm-thick magnetite film (39.9 cm^{-1} [13]), and a 200-nm-thick film with a preferred (111) orientation (41 cm^{-1} [14]).

The signal from the silicon substrate, which is represented by the peak at a frequency of 520 cm^{-1}, decays as the magnetite film grows thicker and vanishes at a thickness of 200 nm. Owing to this, peak $T_{2g}(2)$ of the magnetite film at 538 cm^{-1} becomes easily distinguishable. The FWHM values of this peak were 52.4 and 50.6 cm^{-1} for films with a thickness of 200 and 250 nm, respectively. These widths are close to $\sim$ 48 cm^{-1}, which is the value determined for a bulk magnetite crystal in [15]. It is likely that the values reported in the present study are higher due to the magnetite grains being smaller in size. Specifically, it was found in [16] that the FWHM of the $T_{2g}(2)$ peak is 57.87 cm^{-1} for a 200-nm-thick film with grains 35 nm in size and decreases as grains grow larger.

Figure 2 presents the Raman spectra for films with the lowest thickness (15 and 35 nm). It can be seen that the spectrum for a 15-nm-thick film features a peak at $\sim$ 617 cm^{-1}.

The peak becomes less apparent in the spectrum for a 35-nm-thick film due to an increase in intensity of the adjacent A_{1g}-peak of magnetite. This peak could be attributed to the formation of hematite (α-Fe_2O_3) [17], which is characterized by a peak at a frequency of 615 cm^{-1}. However, an additional more intense peak (E_g) at $\sim$ 414 cm^{-1} from this iron oxide should then be present in the spectrum, but it was not detected. In addition, the formation of hematite is hardly an option, since it should proceed under high oxygen pressures [18]. A peak at a frequency of $610-620$ cm^{-1} is also seen in the Raman spectrum from the surface of pure silicon with orientation (001) [19]. The authors of [20] attributed this
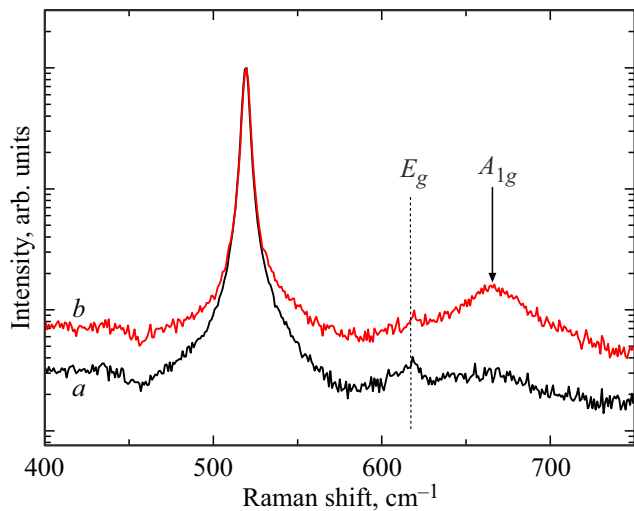
Figure 2. Raman spectra for magnetite films with a thickness of 15 (*a*) and 35 nm (*b*).
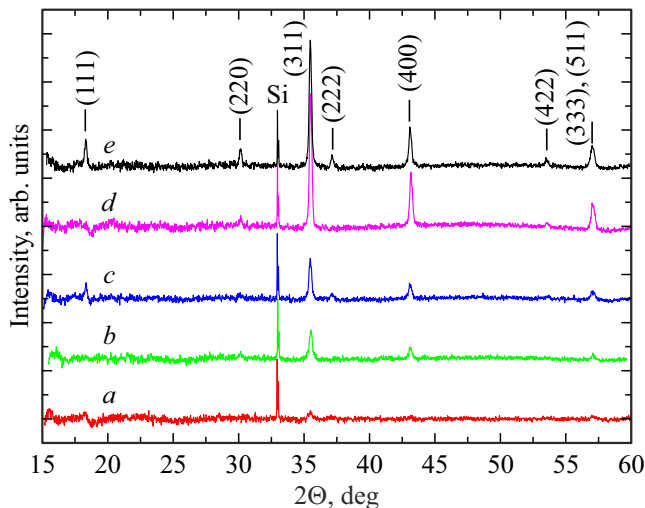
Figure 3. Diffraction patterns for magnetite films with a thickness of 35 (*a*), 70 (*b*), 135 (*c*), 210 (*d*), and 250 nm (*e*) deposited onto the 1.5 nm-SiO₂/Si(001) surface.

peak to a combination of acoustical and optical phonons in the Σ-direction. Thus, the peak at a frequency of $\sim 617\,\mathrm{cm}^{-1}$ in the spectrum for a 15-nm-thick film is likely to be induced by scattering off the Si(001) substrate.

Figure 3 presents the XRD patterns of polycrystalline films of various thickness. With the exception of the forbidden (200) peak from the Si(001) substrate at $2\Theta \approx 32.9^{\circ}$ [21], only magnetite peaks were observed within the range of 2Θ angles from 15 to 60°. As was already noted, RHEED patterns from the film surface reveal a (311) texture [9]. In the case of an ideal uniaxial (311) texture with the [311] axis of the crystallite lattice coinciding with the normal to the film surface (misalignment angle $\varphi = 0^{\circ}$), only Bragg peaks from the system of planes 311, 622, etc., which are parallel to the surface, should be present

in the XRD pattern. According to the Bragg−Brentano geometry, only the crystallites having (hkl)-reflective planes parallel to the sample surface produce contribution to the reflection intensity in the XRD pattern. With an ideal (311) texture, only the (311) planes should be parallel to the sample surface, and a normal to these planes should bisect the angle between incident and reflected X-ray beams. If the (311) texture is non-ideal with $\varphi \neq 0^{\circ}$ (arcs in RHEED patterns indicate that this is the case), certain other planes of misoriented crystallites may align with the surface plane, producing additional Bragg peaks in the XRD pattern. The patterns in Figure 3 do indeed feature peaks complementary to (311). However, the intensity of these peaks should be lower than the corresponding intensity for a film with a completely random orientation of crystallites (powdered magnetite).

The intensities of Bragg peaks both for experimentally grown films and for powdered magnetite [22] are listed in the table. As expected, the majority of Bragg peaks either have a lower intensity (220, 422, and 511/333) than those observed for powder samples or are lacking completely in the XRD patterns for certain thicknesses (e.g., (111) and (222)). The exception is the (400) peak. It is unclear why the intensity of this Bragg peak is so high (higher than 28), since the RHEED patterns reveal that (311) planes have a preferred orientation parallel to the film surface. This may probably be attributed to the fact that the angle between atomic planes (100) and (311) is the smallest (25.2°) compared to all the other planes. In view of this, the probability of scattering off the system of planes (100) in the case of misalignment of crystallites of the (311) texture is higher. At the same time, it is possible that grains with the (100) orientation grow alongside with 311-oriented grains. The coexistence of crystallites of different orientations has also been noted in [23], where magnetron deposition of iron in an oxygen atmosphere was performed. It is possible that the measured RHEED patterns reveal only the (311) texture due to the height of 311 crystallites, which protrude above the surface, exceeding the height of crystallites with the (100) orientation. Since an electron beam is incident at a grazing angle to the surface, transmission diffraction should be limited to (311) crystallites protruding above the surface. The lack (very low intensity) of a (220) peak provides indirect support to the above assumption. Since atomic (110) planes are perpendicular to planes (311) and (100) (and, consequently, the surface), the Bragg condition (in the Bragg−Brentano geometry) for them is not satisfied.

The positions of Bragg peaks for films of various thickness are also listed in the table. It can be seen that these positions are almost independent of the film thickness. This implies that the lattice constant of crystallites does not depend on thickness (at thicknesses above 35 nm).

It follows from the table that the angles of all Bragg peaks exceed the corresponding values for powdered magnetite [22]. The lattice constants of magnetite films were determined using the angle values for the most intense peaks (311, 400, and 511/333). The obtained mean

Intensity and positions of Bragg peaks in the obtained experimental XRD patterns

	(111)	(220)	(311)	(222)	(400)	(422)	(511/333)
Intensity of Bragg peaks							
Fe$_3$O$_4$ [22]	8	28	100	7	21	10	27
35 nm	0	0	100	0	0	0	0
70 nm	0	0	100	0	39.3	0	20.8
135 nm	35	0	100	12	38	0	21
210 nm	0	0	100	0	39.5	2.4	19.5
250 nm	22	12	100	9.5	31	6	18
Positions of Bragg peaks							
Fe$_3$O$_4$ [22]	18.27°	30.09°	35.42°	37.05°	43.05°	53.39°	56.94°
35 nm	–	–	35.48	–	–	–	–
70 nm	–	–	35.45	–	43.09	–	56.96
135 nm	18.32	–	35.47	37.13	43.11	–	57.06
210 nm	–	–	35.50	–	43.17	53.55	57.04
250 nm	18.31	30.13	35.47	37.13	43.12	53.54	57.03
Lattice constant, Å			8.383 ± 0.004		8.381 ± 0.006		8.382 ± 0.006

value $(8.382 \pm 0.005\,\text{Å})$ is approximately 1% lower than the one for bulk magnetite $(8.396\,\text{Å})$. It is interesting to note that a reduced lattice constant value was obtained for both polycrystalline and epitaxial films. Specifically, the maximum lattice constant value determined in [24] for a 68-nm-thick film fabricated under the optimum conditions by magnetron sputtering of Fe was 8.384 Å, and the lattice constant for an epitaxial 150-nm-thick film [13] was 8.382 Å.
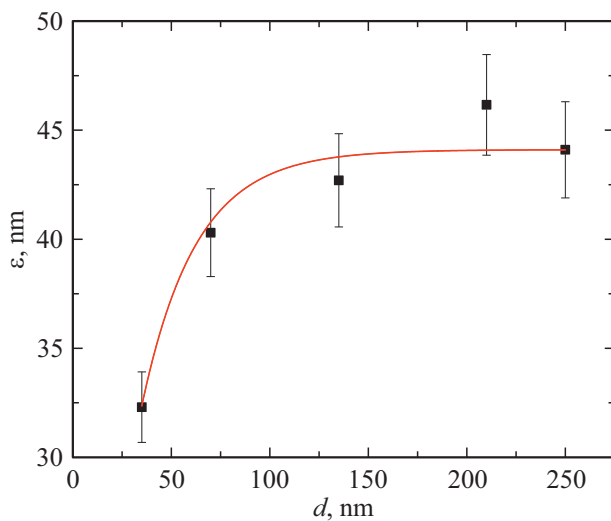
Figure 4. Dependence of the mean crystallite size (ε) calculated in accordance with the Scherrer formula for the (311) peak on the magnetite film thickness (d).

The mean crystallite/grain sizes (ε) were determined using the FWHM values of Bragg peaks. The Scherrer formula was used for this purpose to analyze the (311) peak that was observed starting from a thickness of 35 nm:

$$\varepsilon = \frac{K\lambda}{b \cos \Theta_\text{B}},$$

where ε is the crystallite size, K is the Scherrer constant, λ is the emission wavelength $(1.54\,\text{Å})$, b is the FWHM value (in radians), and Θ_B is the Bragg angle (in degrees). In the case of determination of parameter b from the FWHM (K_w) [25], the Scherrer constant for both cubic and octahedral crystallites assumes a value of approximately 0.9. Figure 4 shows the dependence of the crystallite size on the magnetite film thickness. It can be seen that the maximum mean size of crystallites is close to 45 nm at a film thickness of 250 nm. It is also evident that the crystallite size increases rapidly only up to a thickness of ~ 100 nm (where $\varepsilon = 43$ nm) and varies little as the film thickness grows further (to 250 nm).

As was demonstrated in our earlier study [8] with transmission electron microscopy images, a film with a (311) texture has a columnar structure with iron oxide crystallites growing primarily along the normal to the surface. It is fair to assume that the lateral size of (311) crystallites growing this way (parallel to the surface) should reach a mean constant value at a certain film thickness. Subsequent film deposition should result only in the growth of crystallites along the normal to the surface. The evolution of crystallite size with thickness observed in Figure 4 may be attributed
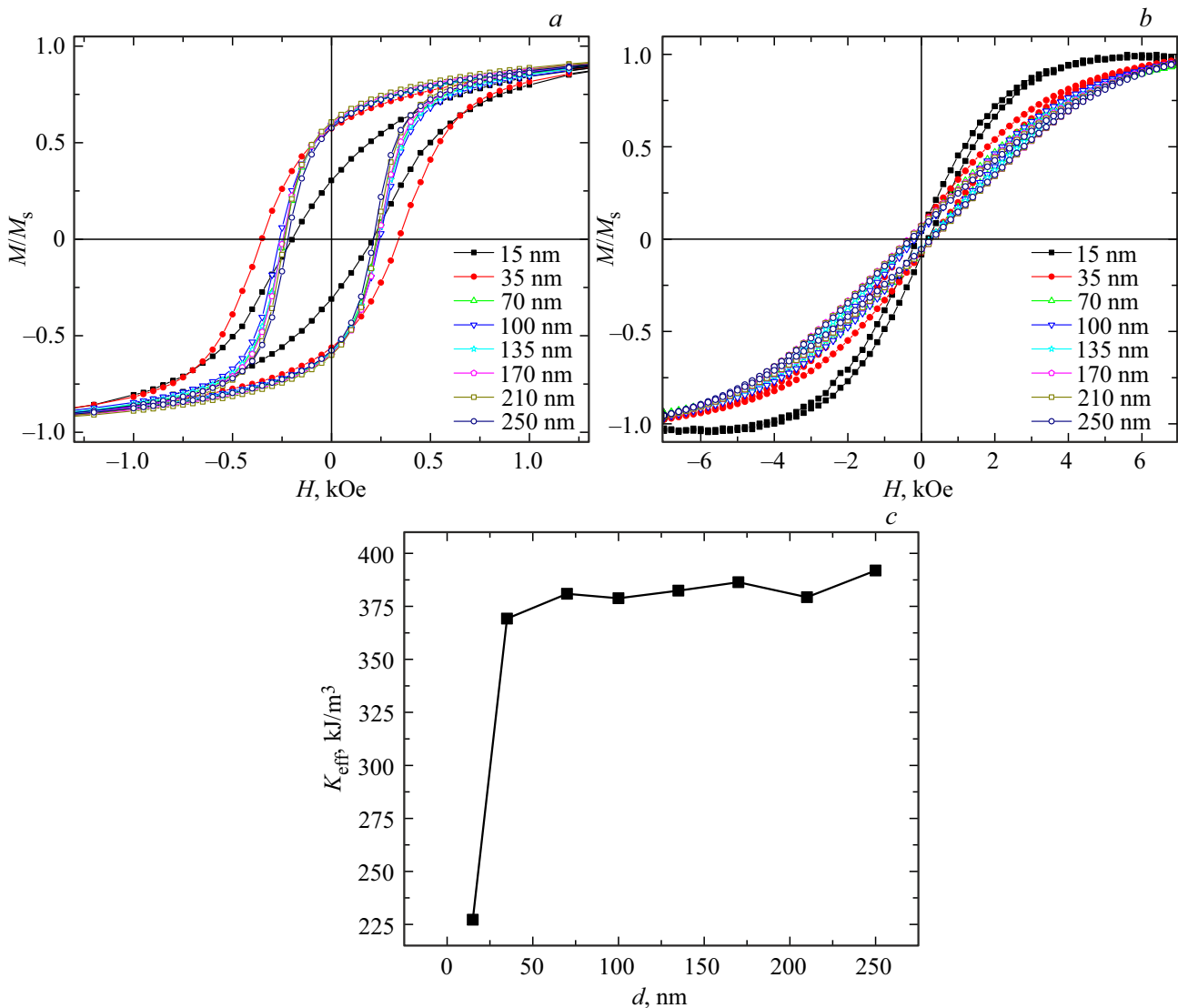
Figure 5. Magnetic hysteresis loops with external magnetic field H being parallel to the sample plane (a) and perpendicular to it (b). Dependence of effective magnetic anisotropy K_{eff} on film thickness d (c).

to a rapid change in the lateral size of magnetite crystals at thicknesses below 100 nm and its insignificant variation in the course of subsequent thickness rise from 100 to 250 nm.

The magnetic properties of samples were examined with external magnetic field H directed parallel to the sample plane and perpendicular to it. The obtained magnetic hysteresis loops are presented in a normalized form in Figure 5. All the studied samples had their easy axis in the film plane and a hard axis in the perpendicular direction.

With H lying in the film plane (Figure 5, a), the magnetic hysteresis loops for samples thicker than 70 nm were characterized by similar loop shapes and close values of $H_c = 235 \pm 10$ Oe and $M_r/M_s = 0.59 \pm 0.01$. As the film thickness dropped to 35 nm, the coercive force increased considerably to $H_c = 345$ Oe with a slightly reduced value of $M_r/M_s = 0.58$. A further reduction in thickness led to a strong reduction of both $H_c = 203$ Oe and $M_r/M_s = 0.3$.

A similar pattern was identified in H directed perpendicular to the film plane (Figure 5, b): similar loop shapes and close values of $H_c = 269 \pm 30$ Oe and $M_r/M_s = 0.07 \pm 0.01$ were observed for samples thicker than 70 nm. When the film thickness decreased to 35 nm in a field directed this way, the loop shape and the values of $H_c = 260$ Oe and $M_r/M_s = 0.06$ changed only slightly. Compared to other samples, the 15-nm-thick sample is characterized by a strong saturation field decay that is accompanied by a reduction of $H_c = 144$ Oe and $M_r/M_s = 0.03$.

This behavior of hysteresis loops is related directly to a change in effective magnetic anisotropy (Figure 5, c). A pronounced planar anisotropy with $K_{eff} = 383 \pm 5$ kJ/m^3 is observed in bulk samples with a film thickness in excess of 70 nm. Shape anisotropy produces the primary contribution to the effective sample anisotropy at such thickness levels. As the thickness fell to $d = 35$ nm, the anisotropy index

decreased moderately to $K_{\text{eff}} = 369\,\text{kJ/m}^3$; when $d = 35\,\text{nm}$ was reached, it dropped sharply to $K_{\text{eff}} = 227\,\text{kJ/m}^3$. The value of K_{eff} is likely to become zero (when the shape anisotropy reaches equilibrium with other anisotropy types) at film thicknesses below $15\,\text{nm}$ and change sign later on. The easy axis will then be oriented perpendicularly to the sample plane, which is typical of thin magnetic films.

4. Conclusion

Polycrystalline magnetite films were grown on the surface of single-crystal silicon, which was coated with an ultrathin SiO_2 layer, by reactive deposition of iron in a molecular oxygen atmosphere. The evolution of the structural and phase composition of magnetite (Fe_3O_4) films was examined within the 15–250 nm thickness range. Raman spectroscopy data demonstrated that the chemical composition of iron oxide films produced under the given reactive deposition conditions corresponds to the magnetite phase; no other phases were detected. The results of X-ray diffraction analysis revealed that films contain crystallites with two preferred orientations. It was found that crystallites grow in size as the film thickness increases and reach a constant level of $\sim 43\,\text{nm}$ at a thickness of $100\,\text{nm}$. The examination of magnetic properties demonstrated that the magnetic behavior changes drastically in samples with a film thinner than 70 nm due to a reduction in the magnitude of effective anisotropy within the sample plane, which has a significant influence on the coercive force and the ratios of residual magnetization to saturation magnetization.

Conflict of interest

The authors declare that they have no conflict of interest

References

[1] Z. Zhang, S. Satpathy. Phys. Rev. B **44**, 13319 (1991).

[2] I. Zutic, J. Fabian, S. Das Sarma. Rev. Mod. Phys. **76**, 323 (2004).

[3] K. Takanashi. Jap. J. Appl. Phys. **49**, 110001 (2010).

[4] S. Sato, R. Nakane, M. Tanaka. Appl. Phys. Lett. **107**, 032407 (2015).

[5] Y. Saito, T. Inokuchi, M. Ishikawa, T. Ajay, H. Sugiyama. AIP Advances **7**, 055937 (2017).

[6] A. Spiesser, Y. Fujita, H. Saito, S. Yamada, K. Hamaya, S. Yuasa, R. Jansen. Appl. Phys. Lett. **114**, 242401 (2019).

[7] Shwetha G. Bhat, P.S. Anil Kumar. AIP Advances **6**, 056308 (2016).

[8] V.V. Balashev, K.S. Ermakov, A.Yu. Samardak, A.V. Ognev, A.S. Samardak, S.V. Komogortsev, M.N. Volochaev, A.S. Tarasov, V.V. Korobtsov. J. Alloys Compd. **815**, 152398(1−8) (2020).

[9] V.V. Balashev, K.S. Ermakov, D.A. Tsukanov, A.Yu. Samardak, A.V. Ognev, A.S. Samardak. J. Alloys Compd. **961**, 170967(1−7) (2023).

[10] V.V. Balashev, V.V. Korobtsov, T.A. Pisarenko, L.A. Chebotkevich. Tech. Phys. **56**, *10*, 1501 (2011)

[11] L.V. Gasparov, D.B. Tanner, D.B. Romero, H. Berger, G. Margaritondo, L. Forro. Phys. Rev. B **62**, *12*, 7939 (2000).

[12] Olga N. Shebanova, Peter Lazor. J. Solid State Chem. **174**, 424 (2003).

[13] D.M. Phase, Shailja Tiwari, Ram Prakash, Aditi Dubey, V.G. Sathe, R.J. Choudhary. J. Appl. Phys. **100**, 123703 (2006).

[14] Shailja Tiwari, R.J. Choudhary, Ram Prakash, D.M. Phase. J. Phys.: Condens. Matter **19**, 176002 (2007).

[15] Rajeev Gupta, A.K. Sood, P. Metcalf, J.M. Honig. Phys. Rev. B **65**, 104430 (2002).

[16] Qisong Sun, Chunfang Wu, Xinchi Fang, Dongmin Zhang, Minggang Zhu, Dewei Zhao, Congmian Zhen, Li Ma, Denglu Hou. J. Magn. Magn. Mater. **536**, 168128 (2021).

[17] Aaron M. Jubb, Heather C. Allen. ACS Appl. Mater. Interfaces **2**, *10*, 2804 (2010).

[18] V.V. Balashev, V.A. Vikulov, T.A. Pisarenko, V.V. Korobtsov. Phys. Solid State **57**, *12*, 2532 (2015).

[19] K. Ochinokura, T. Sekine, E. Matsuura. J. Phys. Chem. Solids **35**, 171 (1974).

[20] P.A. Temple, C.E. Hathaway. Phys. Rev. B **7**, *8*, 3685 (1973).

[21] Peter Zaumseil. J. Appl. Cryst. **48**, 528 (2015).

[22] Natl. Bur. Stand. (U.S.) Monogr., **25**, *5*, 31 (1967).

[23] G. Zhang, C. Fan, L. Pan, F. Wang, P. Wu, H. Qiu, Y. Gu, Y. Zhang. J. Magn. Magn. Mater. **293**, 737 (2005).

[24] Suraj Kumar Singh, Sajid Husain, Ankit Kumar, Sujeet Chaudhary. J. Magn. Magn. Mater. **448**, 303 (2018).

[25] J.I. Langford, A.J.C. Wilson. J. Appl. Cryst. **11**, 102 (1978).

Translated by D.Safin